Mardali, M.; SalimiJazi, H.R.; Karimzadeh, F.; Luthringer, B.; Blawert, C.; Labbaf, S.:
Comparative study on microstructure and corrosion behavior of nanostructured hydroxyapatite coatings deposited by high velocity oxygen fuel and flame spraying on AZ61 magnesium based substrates.
In: Applied Surface Science. Vol. 465 (2019) 614 - 624.
First published online by Elsevier: 17.09.2018

DOI: 10.1016/j.apsusc.2018.09.127
https://dx.doi.org/10.1016/j.apsusc.2018.09.127

Comparative study on microstructure and corrosion behavior of nanostructured hydroxyapatite coatings deposited by high velocity oxygen fuel and flame spraying on AZ61 magnesium based substrates

M. Mardali[a,b*], H.R. SalimiJazi[a], F. Karimzadeh[a], B. Luthringer[b], C. Blawert[b], S. Labbaf[a]

[a] Department of Materials Engineering, Isfahan University of Technology, Isfahan 84156-83111, Iran

[b] Institute of Materials Research, Helmholtz-Zentrum Geesthacht, 21502 Geesthacht, Germany

Abstract

Hydroxyapatite coatings are biocompatible, osteoconductive and create a corrosion resistance surface on magnesium-based implants. Thermal decomposition of HA during thermal spraying limits its application. To overcome the challenges associated with thermal decomposition of HA during thermal spraying, high velocity oxygen fuel spraying with a good thermal stability for HA is proposed. In this work, the traditional flame spraying was compared to high velocity oxy-fuel (HVOF) for HA depositions on magnesium alloy substrates. The effect of process on microstructure, morphology, corrosion behavior and cellular response of HA layers were evaluated. X-ray diffraction analysis showed that the amount of secondary phases in the HVOF deposited sample was less than that in the flame sprayed coatings. Elemental weight percentage of calcium in corroded surfaces was 21% and 34.5% for HVOF and flame sprayed coatings, respectively. Contrary to the results of the electrochemical impedance spectroscopy measurements for HVOF coating performed during the early hours of immersion in the simulated body fluid (SBF), flame sprayed coating exhibited lower corrosion rate after 5 h immersion in SBF solution.

Keywords

Magnesium, Corrosion rate, Hydroxyapatite, HVOF, Flame spraying

1. Introduction

Magnesium (Mg)-based alloys are biodegradable bio-metals which have recently gained great attention [1-3]. High rate corrosion of these interesting alloys is a major challenge. Coating of surface is a way for reduction of the rate of corrosion [4, 5]. Several investigations dealing with Mg-based alloy implants coated with HA are also of interest [2, 6, 7].

Hydroxyapatite (HA) is a well-known bioceramic which is greatly used for a range of biomedical applications, in particular orthopedic [8]. The main problem associated with the application of HA, is its brittle nature, which limits its medical application. Therefore, it is often applied as

composite, coating or bone filler [9, 10]. HA coatings on metallic substrates provides a bioactive fixation with the host bone [11]. A variety of techniques has been employed for HA coatings on metal substrates [12]. Among them, thermal spraying have been widely used for high scale production [13-16].

One of the challenges of thermal sprayed HA coatings is its excessive thermal decomposition during spraying into relatively unstable phases such as tricalcium phosphate (TCP), tetra calcium phosphate (TTCP) and amorphous calcium phosphate (ACP) [17]. However, presence of a certain amount of these phases improve healing conditions, but at an increased level it can cause rapid dissolution in body fluid thus and reduce the corrosion resistance at early time points [18].

High velocity oxygen fuel spraying (HVOF) is one of the thermal spraying methods that possess some advantages over other plasma heat source techniques. In this process, an appropriate proportion of fuel and oxygen are mixed and a high temperature and high-pressure combustion chamber is created. The powders are introduced into this chamber. Then, high-speed particles approach the substrate. The coating is made by spreading of splats. One of the benefits of this technique is low temperature (~3,000 °C) relative to plasma spraying (~10,000 °C) [19]. Therefore, it is expected that HA thermal decomposition problem will be eliminated by using this method. The high pressure generated in the combustion chamber causes high-speed particles stream during coating that makes high adhesion strength. In comparison with traditional flame spraying which uses heat in its process, HVOF uses both heat and pressure [20-21].

To date, only limited comprehensive studies are available on the comparison of microstructure, corrosion rate and the properties of HA coatings produced by HVOF and flame spraying on the Mg alloy substrates. Therefore, the main aim of the current work is to study the microstructure, surface topography, phases composition and corrosion behavior of the HA flame sprayed and HVOF coatings on magnesium substrate.

2. Materials and methods

2.1. Samples preparation

HA powders were synthesized by calcination of bovine bone at 1,200 °C. In order to modify the surface morphology, the synthesized powders were also treated by spray drying. Details of the powders preparation and specifications were given in the previous publication [22].

The chemical composition of the magnesium alloy substrates (AZ61) was Al 5.5%, Zn 1.5%, Mn 0.78%, Si<0.02%, balance Mg The AZ61 alloy sheet was ground by alumina particles (20 meshes). The grit blasted rectangular AZ61 alloy pieces (15×15×5 mm) were cleaned by immersion in a 10%wt/vol NaOH (in double distilled H_2O) at 70 ˚C for 3 min. Then, samples were anodized in a 3 M KOH and 1.3 M $Na_3(PO_4)$ electrolyte solution at 25 ˚C and 70 V using a

DC power supply (5 A, 30 V, IPC-SL20200J, 20 A, 200 V, Iran) for 60 min. Stainless steel was used as cathode. Thermal spray coating performed on the samples and the distance between the two electrodes was 4 cm. Thermal spray process parameters are given in Table 1 and 2.

Table1. Process parameters of flame spraying process

Acetylene	Oxygen	Spray distance	Powder feeding rate	Scan rate	Spray gun
0.5 bar	1.5 bar	10 cm	20 g/min	0.5 m/sec	GTV Unispray, Germany

Table2. Process parameters of HVOF process

Kerosene	Oxygen	Spray distance	Scan rate	Spray gun
24 L/h	850 L/min	35 cm	0.5 m/sec	GTV, K2 Germany

2. 2. Characterization

Phase characterizations of the powders and coatings were performed by X-ray diffraction (XRD) technique using A Bruker, D8 Advance X-ray diffractometer with Cu Kα radiation. The microstructure and morphology of the particles and coatings were characterized by scanning electron microscopy (SEM) equipped with energy dispersive X-ray spectroscopy (EDX) with low accelerating voltage (Bruker Nano GmbH, Germany). Moreover, profilometry tests were carried out to evaluate the surface topography. In this measurement, images were taken from a surface of 14.5×14.5 mm was scanned.

S_a (arithmetical mean height of a line) shows the height difference of each point with the arithmetical mean of the surface. S_a is generally employed to evaluate surface roughness. The parameters were obtained from the following relationship [23]:

$$S_a = \frac{1}{b-a}\int\int_a^b |Z(x,y)|dxdy \qquad (1\text{-}1)$$

Corrosion tests of coatings were performed by electrochemical impedance spectroscopy (EIS) measurement in simulated body fluid (SBF) using a computer controlled potentiostat system. Simulated body fluid (SBF) was prepared according to the composition suggested by Tang [24]. A setup with a working electrode (coated samples with the area of 0.5 cm^2), the counter electrode (a platinum spiral wire) and a reference electrode (saturated Ag/AgCl) was applied. The frequency range was from 30 kHz to 0.1 Hz and the AC signal amplitude was ±10 mV RMS sinusoidal perturbations. The EIS spectra were analyzed using Zview software (Scribner Associates Inc.). Measurements were repeated for three times. The microstructure of the corroded samples was also studied by SEM. The set up for hydrogen evolution test was the same

as the one which was used by Cui et al. [25]. In the hydrogen evolution test, the coated specimens were immersed in SBF for 12 hours. The evolved hydrogen volumes were recorded per 0.5 h.

3. **Results and discussion weight**

3.1. Microstructure Evaluation of Coatings

Cross-sectional microstructures of the deposited layers are shown in Fig 1. The thickness of the HA coating deposited using flame spraying was in the range of 11-19 µm and the anodized layer thickness was in the range of 2-4 µm. The thickness of the HA coating by HVOF process was between 11-27 µm and the anodized layer thickness was between 2-5 µm. The thickness of the anodized samples before thermal spraying was in the range of 10-13.2 µm.
The anodized layer thickness was reduced after thermal spraying processes. The reduction in the HVOF sample was more pronounced than for the flame sprayed coating. High-speed particles in the HVOF process cause more abrasion of the MgO layer during thermal spraying.
Some pores and cracks can be observed in cross-section images. The cracks were created by residual stress within the HA layer [26]. The existence of the thermal expansion coefficient differences between HA coating and magnesium substrate during the cooling of the splats causes the residual stress in the coating and eventually leads to cracks formation. The thicker HVOF coating and the thinner magnesium oxide middle layer in this sample produce more cracks. Pores in a thermal sprayed coating can be due to various factors, such as air bubble detention in the melted droplet during spraying, as well as the presence of void spaces between splats. Although, all of these empty spaces are essential for the application of these types of coatings since the open-pore structure are used for attachment by bone growth.

The morphology of the sample surface is shown in Fig 2. There were many semi-spread splats or un-melted particles in the flame sprayed surface more than in the HVOF. Micro-cracks were originated by the shrinkages during individual solidification of the splats and their cooling. The microcrack density in the flame sprayed coatings is higher than in the HVOF coatings due to higher temperature of the in-flight particles upon impact in the flame spraying. Moreover, HA particles were integrated into the substrate surface, because of using high-pressure streams during HVOF process. Some un-melted particles were observed in both samples.

The line-scan elemental analysis of the cross-sectional microstructures is presented in Fig 3. Three distinguishable levels of Mg concentration can be observed. The low-magnesium level (1) represents the hydroxyapatite layer. The magnesium oxide layer (2) has an average magnesium level, and zone 3 is attributed to the magnesium alloy substrate. The fluctuations in the plots especially in zone 1 represent porosities and cracks within the HA layer. In zone 2 there is a mild increase of magnesium from left to right, indicating element's penetration in the interface of coating and substrate. It is because of the heat received during the thermal spraying process.

Distributions of the elements on the surface were investigated by EDS (Fig 4). In the HVOF coatings, the elements were more uniform than in the flame sprayed coatings. The presence of low amount of magnesium on the surface was due to non-uniform thickness and less coverage of flame sprayed coating in some areas. The atomic percentage of elements on the surface of hydroxyapatite coatings are presented in Table 3. The measured Ca/P ratio for the flame sprayed and the HVOF samples were around 1.7 for both coatings, which shows no significant changes in the chemical composition after spraying.

Table.3. Element percentage on the HA coatings surface

Elements	Flame sprayed coating, at%	HVOF coating, at%
O	69.7	73.2
Mg	11.5	-
Ca	11.3	16.9
P	6.5	9.9
Al	1.0	-

3.2. XRD phase characterization

Phase compositions of the coatings are shown by XRD patterns in Fig 5. In the HVOF deposited layer, HA was the dominant phase (HA 96.2%, Mg 2.6% and tri-calcium phosphate-TCP 1.2%). In the flame sprayed coating maximum amount of the formed phases was HA (HA 61.8%, Mg 25.9%, TCP 6.9%, and MgO 5.4%).

In the HVOF technique, the intermediate phases of calcium phosphate were less than that of the flame spraying. This can be attributed to the lower temperatures and higher speeds of particles. In fact, the particles have a lower residence time in the flame and therefore do not completely melt. However, in the flame spraying, due to the longer time of residence in the flame, complete melting of particles and subsequent recrystallization occur. Semi-stable phases were formed during the recrystallization of the melted particles.

Decomposition of the HA phase includes three stages, a) water evaporation b) dehydroxylation, and c) phase transformation. Beta and alpha tri-calcium phosphate, tetra calcium phosphate and calcium oxide are products of HA decomposition with increasing temperature. In this spectrum, the rate of solubility of the phases decreases in the physiological solution of the body, respectively [27]. The relationship between the increase of solubility and bioactivity is well known. Thus, it is expected that the flame sprayed coating is more bioactive with a higher percentage of the intermediate phases.

3.3. Surface roughness

The two light scanning microscopy patterns for the HA coatings produced by flame spraying and HVOF are shown in Fig 6. The average roughness, S_a, obtained from profilometer analyses and measured using Eq. 1-1, are presented in Table 4. High degree of roughness in the bare alloy was due to the grit blasting before anodizing. Such surface roughness could increase the mechanical interlocking between the coating and the substrate, making them more adhesive. No significant changes in the roughness after anodizing were measured. In Table 4, a S_a of 6 μm and 10.2 μm were calculated for HVOF and flame sprayed coatings, respectively. The high velocity of the in-flight particles in the HVOF method is the main factor for its low roughness.

The surface roughness of the HVOF coatings were reduced compared to the anodized surface due to the high-speed particles impacted on the surface. Flame spraying process did not have any significant influence on the roughness of the coatings.

It is known that bone tissue growth becomes more intense within a rough surface. In fact, micro-rough surface can be beneficial for biosynthesis and adherence to surrounding tissue [8]. On the other hand, increase of the surface roughness results in a higher corrosion rate [28]. Therefore, it can be expected that the flame sprayed coating with higher roughness is more bioactive than the HVOF coating. However, with increasing of contact areas with the corrosive solution, corrosion resistance of this coating is reduced.

Table4. Analytical results of the profilometer tests

Sample	S_a (μm)
AZ61 alloy	9
Anodized	9.2
HVOF	6
Flame sprayed	10.2

3.4. Corrosion tests

3.4.1. Electrochemical impedance spectroscopy measurements

EIS was used to compare the impedance of the samples in SBF solution at 37 °C after 3 h (Fig 7). The double-loop pattern was seen in the nyquist plots. Resistance at high frequencies is related to the defects at the substrate-coating interface (charge transfer resistance). The diameter of the loop in this region demonstrates the size of the transfer resistance (R_{ct}). The second loop at lower frequencies is attributed to the resistance of ceramic coating (R_{pore}).

The diameter of semicircles in the nyquist diagram has a direct relation to the corrosion resistance of the samples. A higher magnitude for the HA-coated samples compared to the bare

and anodized specimen indicates an increase in the corrosion resistance of the HA coated specimens. Higher impedance at lower frequencies shows more corrosion resistance.

Fig 7(a) shows that R_{pore} of the anodized sample equals to R_{ct} of the HA coating plus anodized samples. The nyquist curves obtained from EIS tests were fitted by the Z-view software. Values of the characterized elements for the samples are presented in Table 5. Calculated R values for the hydroxyapatite-coated samples were much higher than the anodized sample, which indicates the effect of HA coating on the reduction of corrosion rate. In addition, the resistance value for the HVOF sample was greater than that of the flame sprayed after 3 h immersion in the SBF solution.

CPE_{ct} is constant phase element capacitance related to the intact coating. Its magnitude represents dielectric constant of the coating. Larger CPE_{ct} means that solution leaks inside the coating. CPE_{ct} and R_{pore} are related inversely [29].

Table.5.Electrochemical corrosion parameters of the AZ61, flame spray and HVOF samples

Sample	R_s (Ωcm^2)	R_{pore} (Ωcm^2)	R_{ct} (Ωcm^2)	CPE_{dl}-T ($10^{-3}Fcm^{-2}$)	n_{dl}	CPE_{ct}-T ($10^{-5}Fcm^{-2}$)	n_{ct}
Anodized alloy	37.88 ± 1.3	141.3 ± 1.6	91.06 ± 3.5	1.74 ± 0.12	0.87 ± 0.06	2.35 ± 0.008	0.85 ± 0.03
HVOF	47.43 ± 2	266.9 ± 2.1	305.2 ± 1.3	1.38 ± 0.5	0.83 ± 0.04	1.53 ± 0.68	0.87 ± 0.05
Flame spray	38.24 ± 0.9	284.7 ± 3.4	274.1 ± 2	0.87 ± 0.06	0.84 ± 0.5	1.54 ± 0.04	0.85 ± 0.03

As shown in Fig 7 and Table 5, the instantaneous impedance of HVOF was slightly higher than that for the flame sprayed sample after 3 hours immersion. However, the important point is that impedance changes over time.

Fig 8 presents the variations of both coatings. In the flame sprayed sample, the impedance increased with the passing time, which could be an indication of a gradual formation of a protective layer from corrosion products on the surface. The corrosion products created a layer on the specimen, which prevents the solvent-to-surface contact and increasing corrosion resistance. Failure of the passive layer was not observed in this sample. While, in the HVOF plot, the impedance was gradually reduced after 3 h, which indicates that the protective layer was broken.

Microstructure and analysis of the corroded surfaces are shown in Fig 9. Compared to the non-corroded coating microstructure in Fig 2 cracks networks can be seen on the surface. In Fig. 9b, the surface morphology is indicative of the inflation of the coating during hydrogen release. Pitting and localized corrosion of the magnesium-based substrate are observed in the areas where

the solution has reached the substrate. The formed calcium phosphate precipitations on the pitting and cracks are shown. Cauliflower-like structure precipitations formed on the surface of the HA coatings in the flame sprayed sample (Fig 9(c)). In the HVOF specimen, more cracks can be observed and the number of precipitated particles was less than that on the flame sprayed coatings (Fig 9(d)). The Ca/P ratio on the surface of the Mg alloy, anodized sample and HA coatings deposited by HVOF and flame spraying were measured using elemental analysis. They were respectively 2.08, 0.81, 1.65 and 3.87. The increase in this ratio shows the presence of more calcium ions on the surface, indicating more calcium phosphate formation. These ions were precipitated on the surface due to the dissolution of the calcium phosphate coating in the solution and their re-depositing on the surface or direct precipitation of calcium and phosphate ions from SBF. On the other hand, hydroxyapatite coating surface initially has negative potential and this causes absorption of calcium ions from the liquid. An increase of calcium content can influence on the conversion of hydroxyapatite to the amorphous phase (ACP). In this stage, the Ca/P ratio increases. As a result, the sample surface has more positive potential and absorbs HPO_4^{2-} ions. Then, the ratio of calcium to phosphorus will be reduced. These processes take place within 6 to 9 h. Thus, pseudo-bone apatite forms from crystallization of the amorphous phase by absorbing ions present in the solution on the surface [30].

Because of the less instability of phases in the flame sprayed sample, the coating is more rapidly dissolved in the solution, and thus more calcium ions are formed around the surface. These ions in the next step and with the rise of pH have the ability to resorb on the surface, which creates a protective layer on the surface. The HVOF coating contains a higher percentage of hydroxyapatite crystalline phases with higher chemical stability that is responsible for higher corrosion resistance at initial times. The presence of cracks in the coating causes corrosion of the substrate over time. The lack of enough calcium ions and the proper conditions for the formation of a protective layer from corrosion products cause the gradual loss of its corrosion resistance.

3.4.2. Hydrogen evolution test

The amount of evolved hydrogen gas, as a corrosion byproduct during immersion in SBF at ambient temperature, is shown in Fig 10. The amount of H_2 gas outlet rate of the uncoated magnesium alloy is much higher than for the coated samples, which shows the highest corrosion rate. The minimum amount of the released H_2 belongs to the flame sprayed sample.

By visual inspection of the corroded surfaces after hydrogen evolution test, it is clear that large cracks and cavities can be observed on the surface of the magnesium alloy, which could be the results of pitting and localized corrosion (Fig 11). The difference in the corroded samples is the appearance of white precipitations as corrosion products (or un-corroded HA coating) and fresh magnesium surface. On the flame sprayed sample, pitting effect and cracks are less numerous.

4. Conclusion

An investigation on the microstructural characterization and corrosion performance of HA coatings deposited by flame spraying and HVOF were performed in this work. Taken the results all together, HVOF coatings had more stable phases, more cracks and less roughness compared to the flame sprayed coating. The EIS measurements in the early stage showed that corrosion resistance of the HVOF was higher than flame sprayed coatings. However, the presence of more cracks in this sample resulted in leaking of SBF solution to the underlying substrate over time, intensifying corrosion. However, in the flame sprayed samples, corrosion products formed a protective layer that increased corrosion resistance over time. It is likely that presence of more intermediate phases in the coating facilitated the formation of a protective layer of pseudo bone apatite.

It was previously shown in literature that RF-magnetron sputtering is also capable of significant improvement of Mg-alloys corrosion resistance [31]. The coatings obtained in literature are single-phase and pore free. At this work, the single phase is HA. This phase is more stable regarding other Ca-P phases. However, the presence of some more unstable phase, such as beta-TCP increases the surface bioactivity, which reduces the time required for bone repair. On the other hand, as it was seen in the current work, the higher amount of unstable phases in the flame sprayed coating contributes to the overall corrosion resistance of the magnesium substrate over time. Moreover, the presence of some pores in coatings for implants applications can be beneficial. The open-pore structure can improve the attachment of bone cells to the implant. In comparison to the published literature, the innovation of this work is to investigate the impedance and corrosion behavior of such a coating over time.

Acknowledgements

The financial support received from Isfahan University of Technology of Iran and Helmholtz Zentrum Geesthacht of Germany is acknowledged.

References

[1] M. Razavi, M. Fathi, O. Savabi, B. HashemiBeni, S. M. Razavi, D. Vashaee, L.Tayebi, Coating of biodegradable magnesium alloy bone implants using nanostructured diopside ($CaMgSi_2O_6$), Appl. Surf. Sci. 1 (2014) 130-137.

[2] J.H.Gao, S.K.Guan, J.Chen, L.G.Wang, S.J.Zhu, J.H.Hu, Z.W.Ren, Fabrication and characterization of rod-like nano-hydroxyapatite on MAO coating supported on Mg–Zn–Ca alloy, Appl. Surf. Sci. 257 (6) (2011) 2231-2237.

[3] A. A.Ghoneim, A. M.Fekry, M. A. Ameer, "Electrochemical behavior of magnesium alloys as biodegradable materials in Hank's solution, Electrochim Acta. 55 (20) (2010) 6028-6035.

[4] Y. B. Zhao, H. P. Liu, C. YangLi, Y. Chen, S. Q. Li, R. C. Zeng, Z. L. Wang, Corrosion resistance and adhesion strength of a spin-assisted layer-by-layer assembled coating on AZ31 magnesium alloy, Appl. Surf. Sci. 434 (2018) 787-795.

[5] S. Heise, M. Höhlinger, Y. Torres Hernández, J. J. PavónPalacio, J. A. Rodriquez Ortiz, V. Wagener, S. Virtanen, A.R. Boccaccin, Electrophoretic deposition and characterization of chitosan/bioactive glass composite coatings on Mg alloy substrates, Electrochim Acta.232 (2017) 456-464.

[6] S. T. Jiang, J. Zhang, S. Z. Shun, M. F. Chen, The formation of FHA coating on biodegradable Mg-Zn-Zr alloy using a two-step chemical treatment method, Appl. Surf. Sci. 388 (A) (2016) 424-430.

[7] A. Zomorodian, C. Santos, M.J. Carmezim, T. Moura e Silva, J.C.S. Fernandes, M.F. Montemor, In-vitro" corrosion behavior of the magnesium alloy with Al and Zn (AZ31) protected with a biodegradable polycaprolactone coating loaded with hydroxyapatite and cephalexin, Electrochim Acta. 179 (2015) 431-440.

[8] D. O. Costa, P. D. Prowse, T. Chrones, S. M. Sims, D. W. Hamilton, A. S. Rizkalla, S. J. Dixon, The differential regulation of osteoblast and osteoclast activity by surface topography of hydroxyapatite coatings, Biomaterials. 34 (30) (2013) 7215–7226.

[9] M. B. Kannan, Hydroxyapatite coating on biodegradable magnesium and magnesium-based alloys, *Hydroxyapatite (HAp) for Biomedical Applications*, Elsevier, 2015, pp. 289–306.

[10] S. R. Kiahosseini, A. Afshar, M. Mojtahedzadeh Larijani, M. Yousefpour, Structural and corrosion characterization of hydroxyapatite/zirconium nitride-coated AZ91 magnesium alloy by ion beam sputtering, Appl. Surf. Sci. 401 (2017) 172-180.

[11] M. H. Uddin, A. Nakahira, M. Okazaki, T. Sohmura, and T. Matsumoto, *Biomimetic Fabrication of Apatite Related Biomaterials*. INTECH Open Access Publisher, 2010.

[12] A.Yanovska, V.Kuznetsov, A.Stanislavov, S.Danilchenko, L.Sukhodub, Calcium–phosphate coatings obtained biomimetically on magnesium substrates under low magnetic field, Appl. Surf. Sci. 258 (22) (2012) 8577-8584.

[13] H. Li, K. A. Khor, and P. Cheang, Thermal sprayed hydroxyapatite splats: nanostructures, pore formation mechanisms and TEM characterization, Biomaterials. 25 (17) (2004) 3463–3471.

[14] H. Li, K. A. Khor, and P. Cheang, Impact formation and microstructure characterization of thermal sprayed hydroxyapatite/titania composite coatings, Biomaterials. 24 (6) (2003) 949–957.

[15] K. Khor, H. Li, and P. Cheang, Processing–microstructure–property relations in HVOF

sprayed calcium phosphate based bioceramic coatings, Biomaterials. 24 (13) (2003) 2233–2243.

[16] S. W. Kweh, K. Khor, P. Cheang, An in vitro investigation of plasma sprayed hydroxyapatite (HA) coatings produced with flame-spheroidized feedstock, Biomaterials. 23 (3) (2002) 775–785.

[17] K. A. Khor, H. Li, P. Cheang, Significance of melt-fraction in HVOF sprayed hydroxyapatite particles, splats and coatings, Biomaterials. 25 (2004) 1177–1186.

[18] F. Feyerabend, In vitro analysis of magnesium corrosion in orthopaedic biomaterials, Biomaterials for Bone Regeneration, Elsevier, 2014, pp. 225–269.

[19] L. Fedrizzi, S. Rossi, R. Cristel, P.L. Bonora, Corrosion and wear behaviour of HVOF cermet coatings used to replace hard chromium, Electrochim Acta. 49 (2004) 2803-2814.

[20] R. S. Lima, K. A. Khor, H. Li, P. Cheang, and B. R. Marple, HVOF spraying of nanostructured hydroxyapatite for biomedical applications, Mater. Sci. Eng. A. 396 (2005) 181–187.

[21] M. Oksa, E. Turunen, T. Suhonen, T. Varis, and S.-P. Hannula, Optimization and Characterization of High Velocity Oxy-fuel Sprayed Coatings: Techniques, Materials, and Applications, Coatings. 1 (2) (2011) 17–52.

[22] M. Mardali, H. SalimiJazi, F. Karimzadeh, B. Luthringer, C. Blawert, S. Labbaf, Fabrication and characterization of nanostructured hydroxyapatite coating on Mg-based alloy by high-velocity oxygen fuel spraying, Ceram. Int. 44 (12) (2018) 14667-14676. doi.org/10.1016/j.ceramint.2018.05.093

[23] E. S. Gadelmawla, M. M. Koura, T.M.A. Maksoud, I. M. Elewa, H.H. Soliman, "Roughness parameters, J. Mater. Process. Technol. 123 (2002) 133-145.

[24] H. Tang, D.Z. Yu, Y. Luo, F.P. Wang, Preparation and characterization of HA microflowers coating on AZ31 magnesium alloy by micro-arc oxidation and a solution treatment, Appl. Surf. Sci. 264 (2013), 816-822.

[25] L. -Y. Cui, Y. Hu, R. -C. Zeng, Y. -X. Yang, D. -D. Sun, S. -Q. Li, F. Zhang, E. -H. Han, New insights into the effect of Tris-HCl and Tris on corrosion of magnesium alloy in presence of bicarbonate, sulfate, hydrogen phosphate and dihydrogen phosphate ions, j. Mater. Sci. Technol. 33 (9) (2017) 971-988.

[26] H. D. L. Robert B. Heimann, Wiley: Bioceramic Coatings for Medical Implants: Trends and Techniques - Robert B. Heimann, Hans D. Lehmann, 2015.

[27] C. C. Chena, T.H. Huanga, C.T. Kaoa, S.J. Ding, Electrochemical study of the in vitro degradation of plasma-sprayed hydroxyapatite/bioactive glass composite coatings after heat treatment, Electrochim Acta. 50 (2004) 1023-1029.

[28] R. Walter, M. Bobby Kannan, Influence of surface roughness on the corrosion behaviour of magnesium alloy, Mater. Des. 32, (4) (2011) 2350-2354.

[29] M. Razavi, M. Fathi, O. Savabi, B. Hashemi Beni, D. Vashaee, L. Tayebi, Nanostructured merwinite bioceramic coating on Mg alloy deposited by electrophoretic deposition, Ceram. Int. 40 (2014) 9473-9484.

[30] C. C. Berndt, F. Hasan, U. Tietz, and K.-P. Schmitz, A Review of Hydroxyapatite Coatings Manufactured by Thermal Spray, in Advances in Calcium Phosphate Biomaterials, B. Ben-Nissan, Ed. Berlin, Heidelberg: Springer Berlin Heidelberg, 2014, pp. 267–329.

[31] T.M. Mukhametkaliyev, M.A. Surmeneva, A. Vladescu, C.M. Cotrut, M. Braic, M. Dinu, M.D. Vranceanu, I. Pana, M. Mueller, R.A. Surmenev, A biodegradable AZ91 magnesium alloy coated with a thin nanostructured hydroxyapatite for improving the corrosion resistance, Mater Sci Eng C. 75 (2017) 95–103.

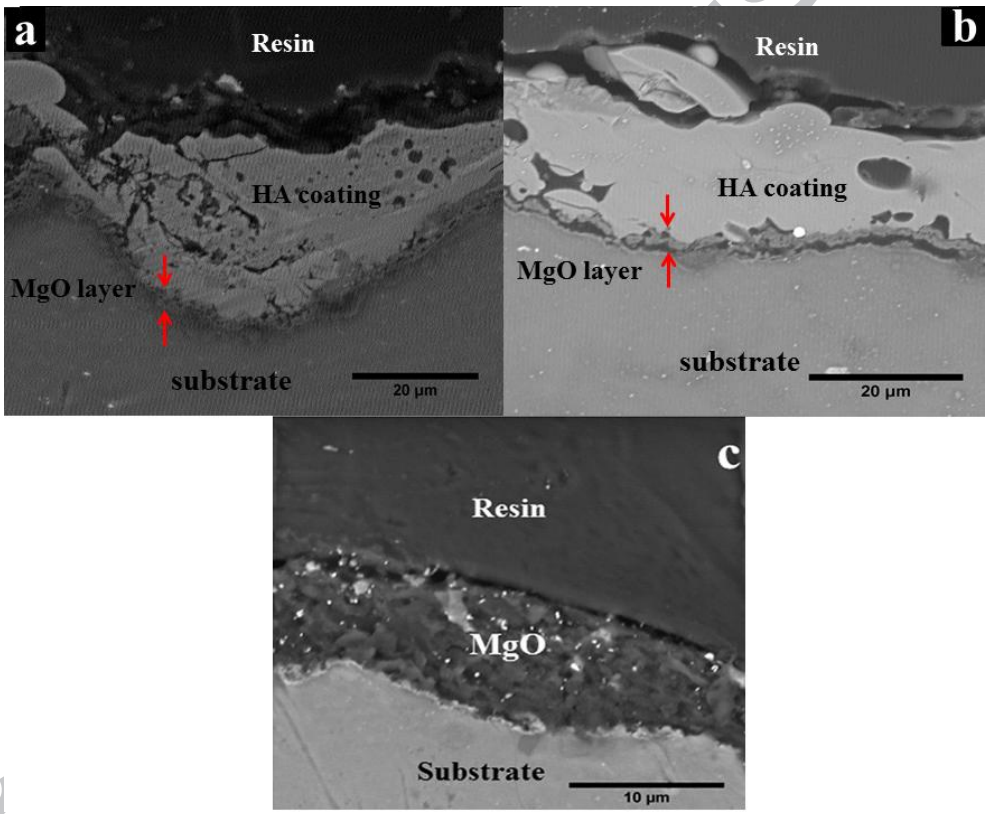

Fig.1. Cross-sectional microstructure of the a) HVOF, b) Flame sprayed and c) Anodized sample

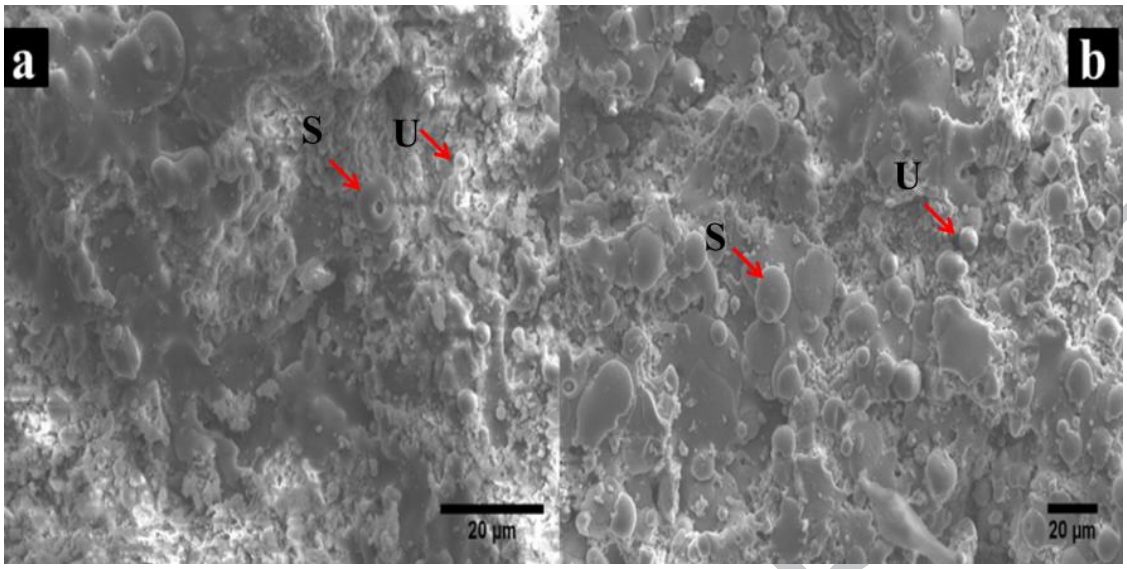

Fig.2. Microstructure of the surface of HA coating deposited by a) HVOF and b) Flame spraying (S: semi spread splats, U: un-melted particles

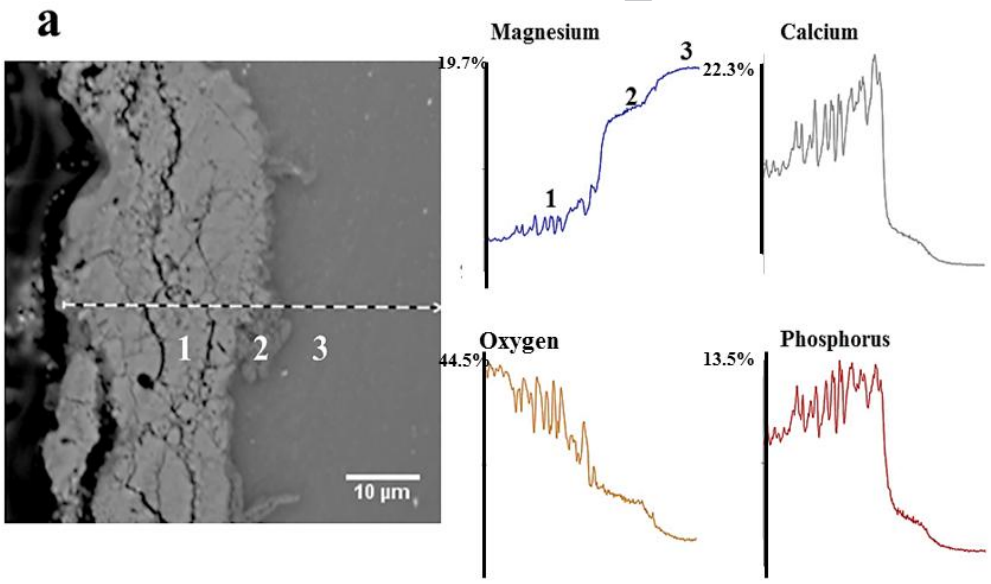

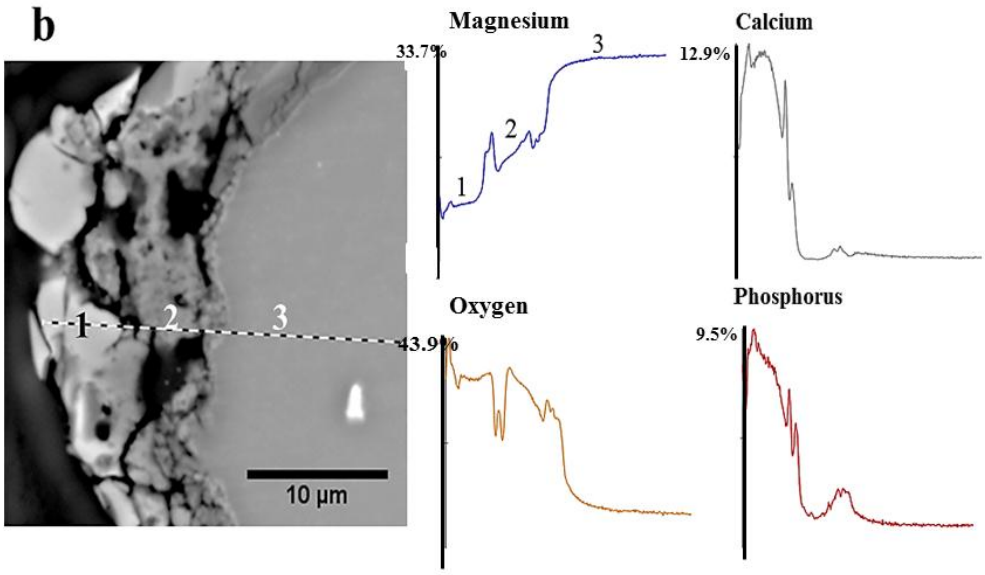

Fig.3. Line-scan elemental analysis of a) HVOF and b) Flame sprayed coatings

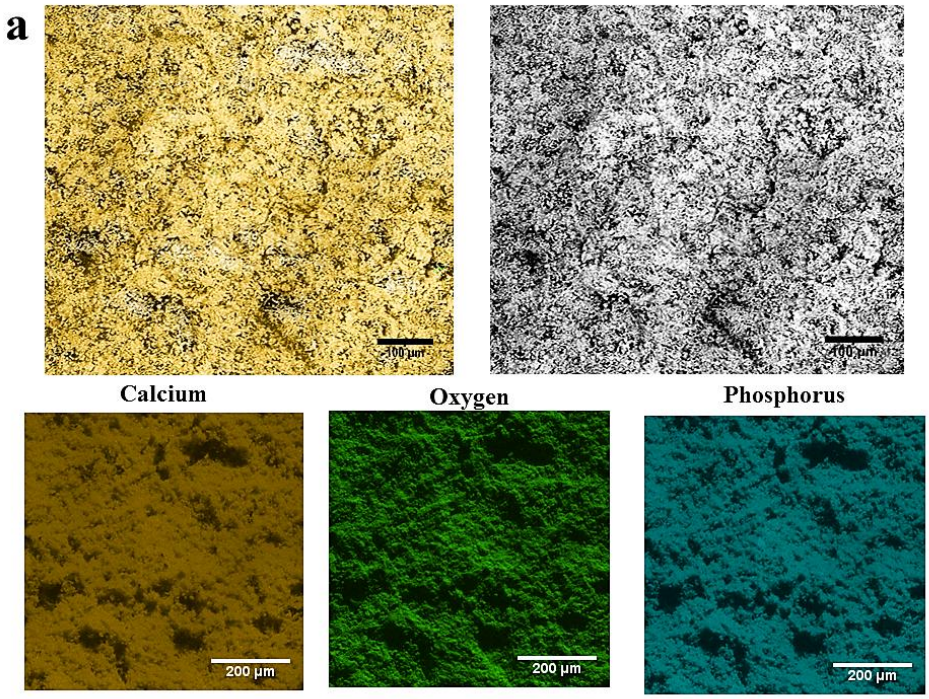

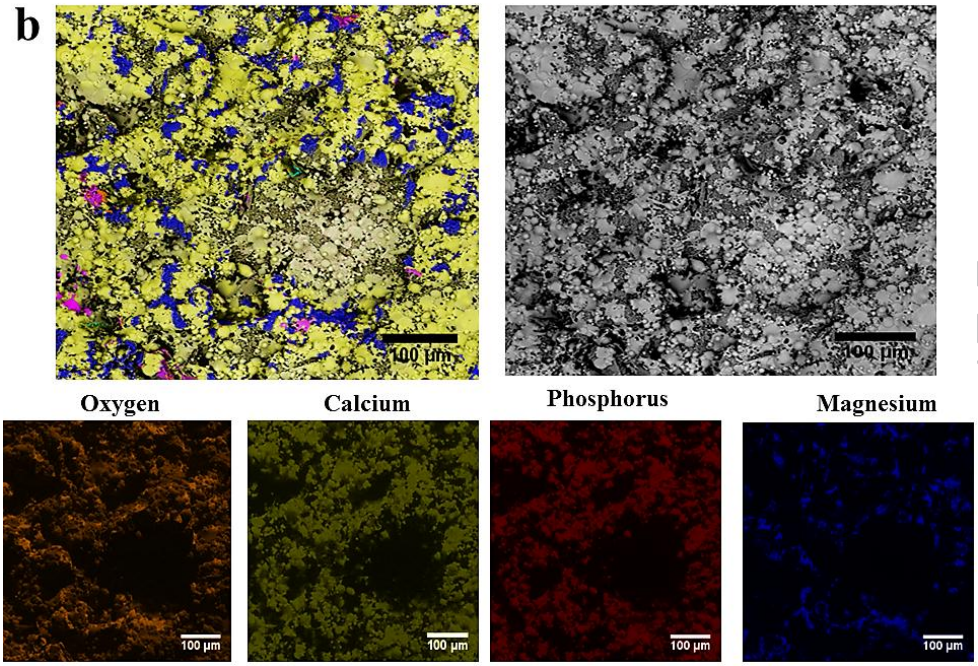

Fig.4. Elemental map analysis of a) HVOF and b) Flame sprayed coatings

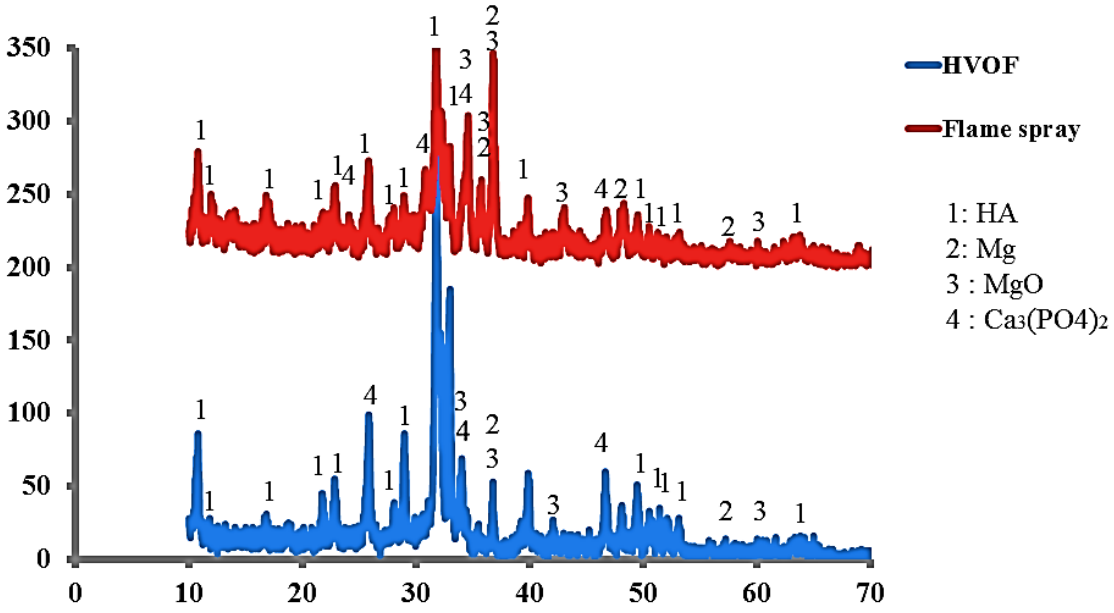

Fig.5. XRD patterns of the anodized plus HA layer deposited by HVOF and flame spraying

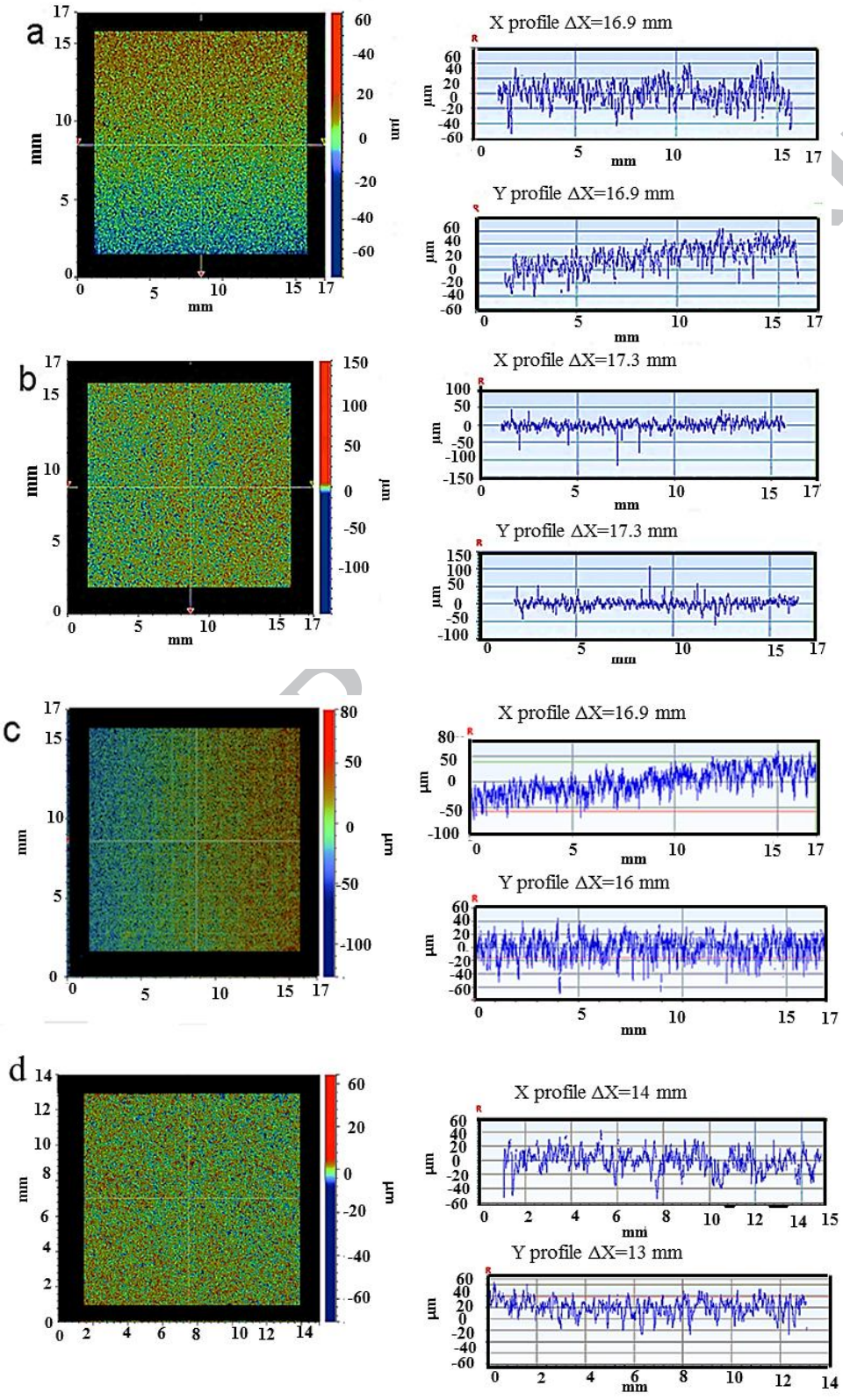

Fig.6. Profilometer patterns of a) Bare alloy, b) HVOF, c) Flame sprayed surface and d) Anodized samples

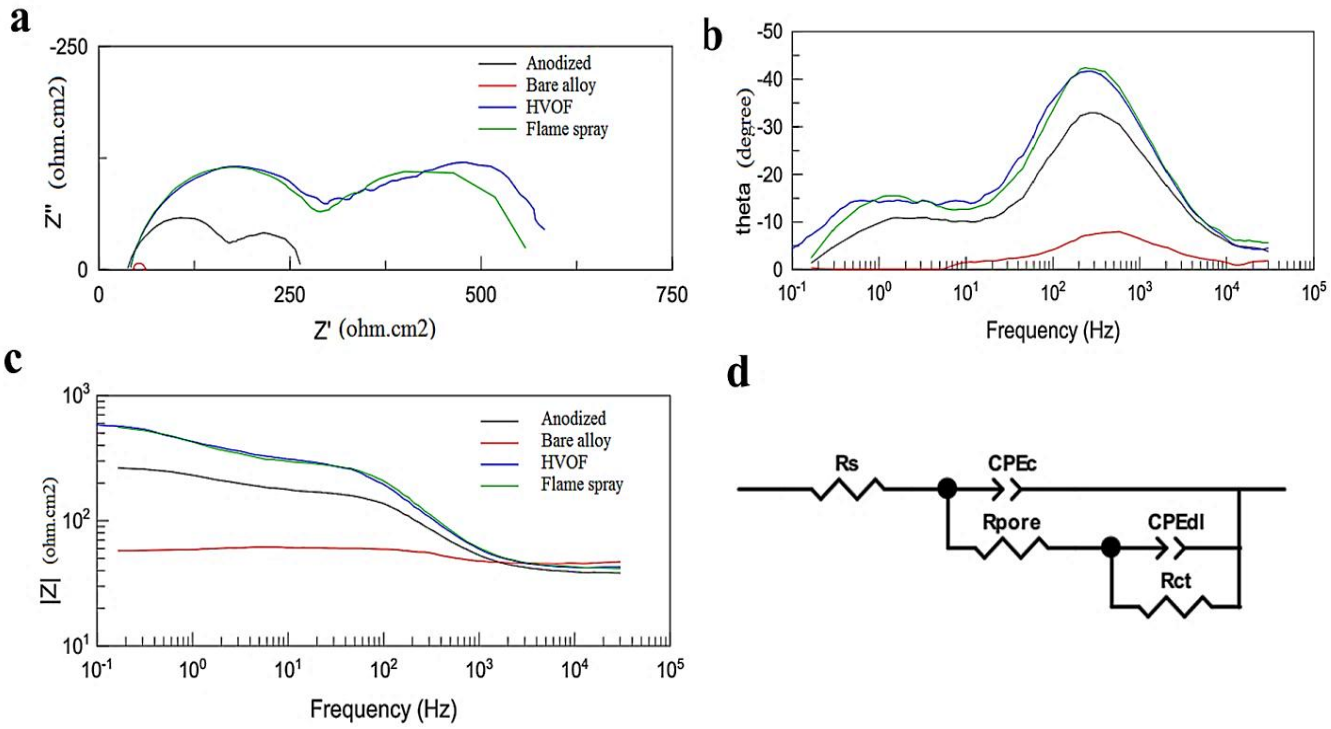

Fig.7. Plots of EIS tests a) nyquist plots, b and c) Bode plots and d) equivalent circuit for modeling

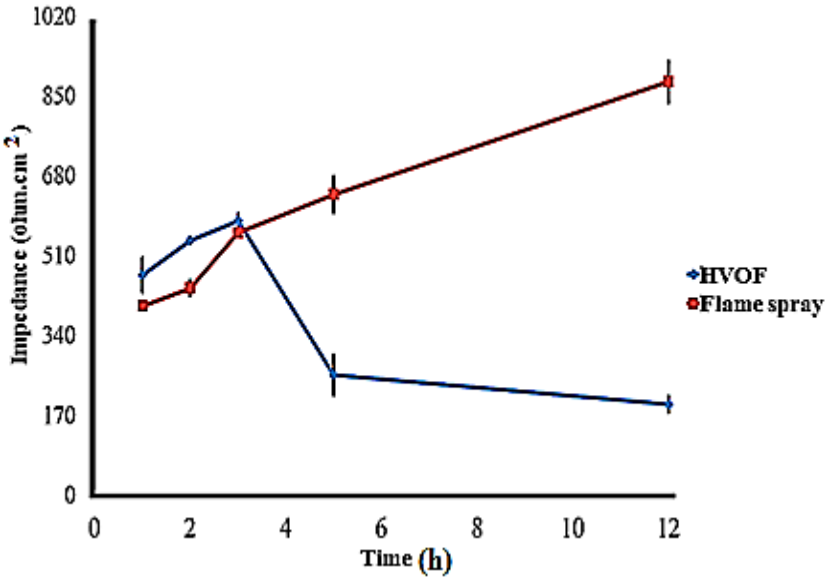

Fig.8. Variations in impedance of the HVOF and flame sprayed coatings during 12 hours immersion in SBF solution at 0.1 (Hz)

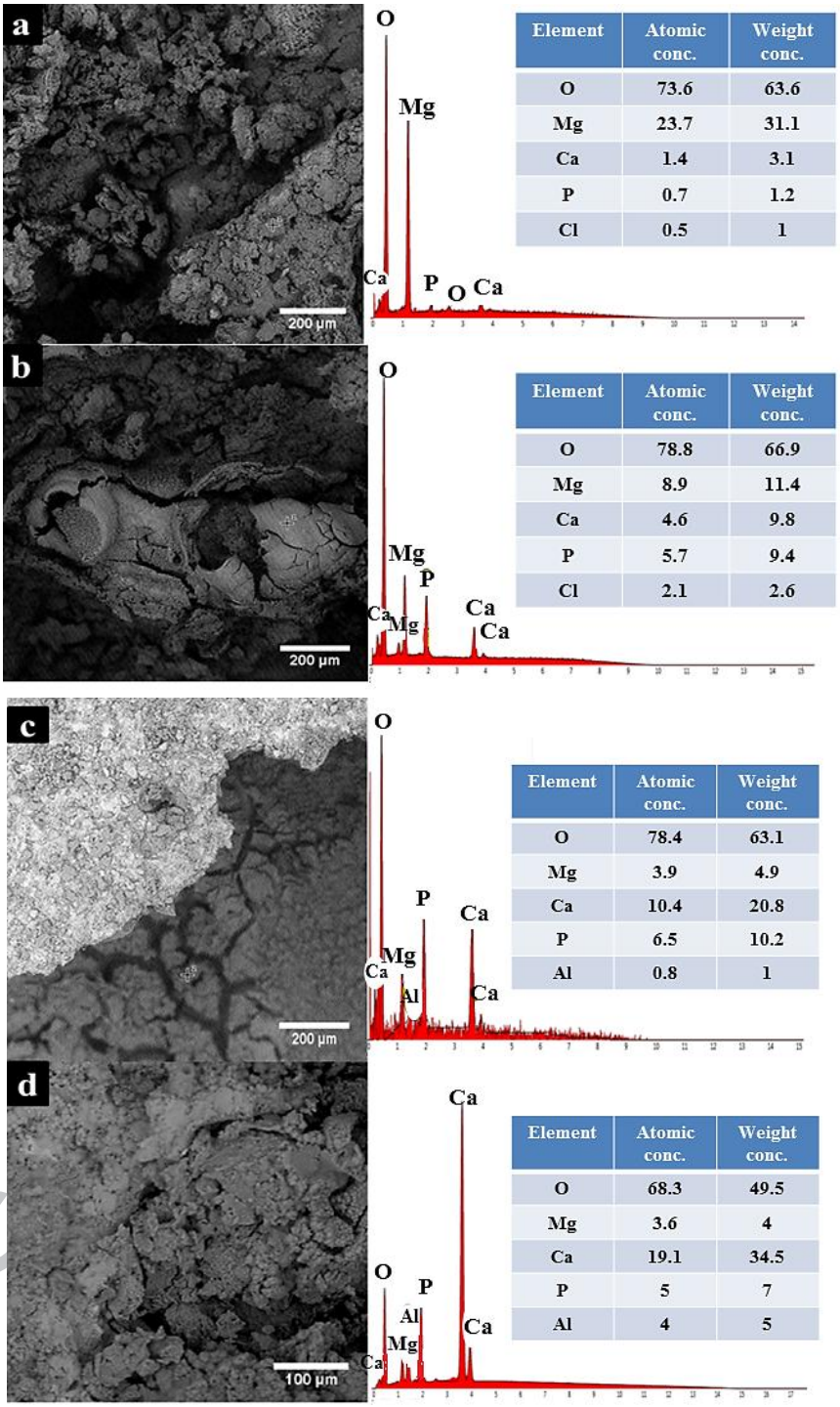

Element	Atomic conc.	Weight conc.
O	73.6	63.6
Mg	23.7	31.1
Ca	1.4	3.1
P	0.7	1.2
Cl	0.5	1

Element	Atomic conc.	Weight conc.
O	78.8	66.9
Mg	8.9	11.4
Ca	4.6	9.8
P	5.7	9.4
Cl	2.1	2.6

Element	Atomic conc.	Weight conc.
O	78.4	63.1
Mg	3.9	4.9
Ca	10.4	20.8
P	6.5	10.2
Al	0.8	1

Element	Atomic conc.	Weight conc.
O	68.3	49.5
Mg	3.6	4
Ca	19.1	34.5
P	5	7
Al	4	5

Fig.9. Microstructure of the corroded samples a) bare alloy, b) anodized, c) flame sprayed and d) HVOF sample after 3 h in SBF

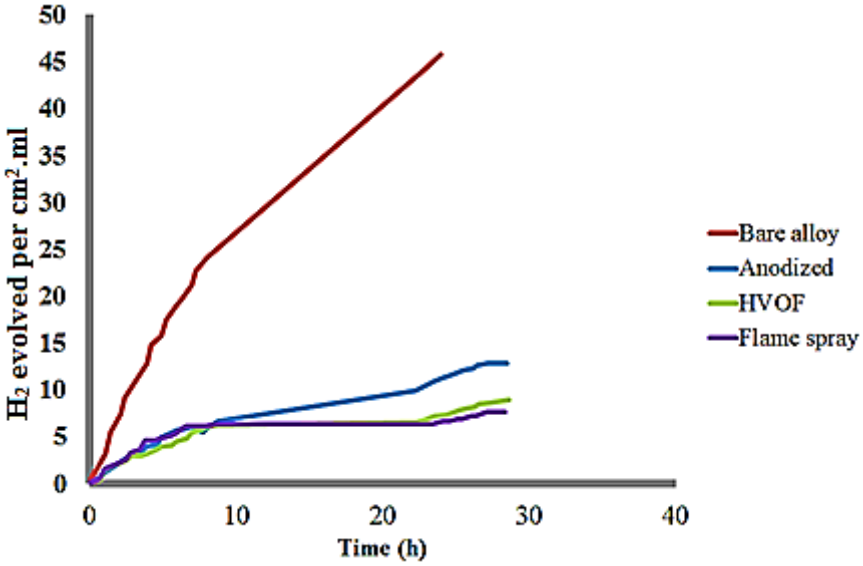

Fig.10.Evolved hydrogen gas during corrosion of samples in SBF

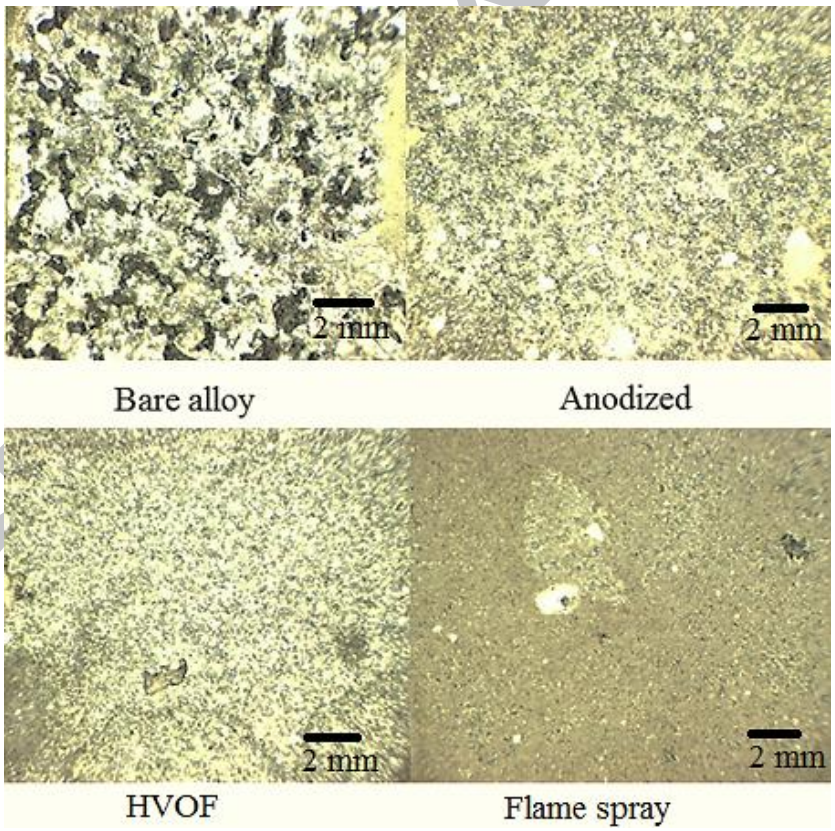

Fig.11. Optical microscopic images of the samples after immersion time in SBF solution

Highlights

“Comparative study on microstructure and corrosion behavior of nanostructured hydroxyapatite coatings deposited by high velocity oxygen fuel and flame spraying on AZ61 magnesium based substrates”

- HVOF coatings had more stable phases, more cracks and less roughness compared to the flame sprayed coating
- The corrosion resistance of the HVOF was higher than flame sprayed coatings
- In the flame sprayed samples, corrosion products formed a protective layer that increased corrosion resistance over time